The Canadian Mineralogist
Vol. 46, pp. 1215-1233 (2008)
DOI: 10.3749/canmin.46.5.1215

THE MANGANESE DEPOSITS OF THE PAMPEAN RANGES, ARGENTINA

PABLO RODRIGO LEAL[§]

Department of Geology, University of Buenos Aires, Ciudad Universitaria, Pabellón II, C1428EHA, and Consejo Nacional de Investigaciones Científicas y Técnicas (CONICET), Buenos Aires, Argentina

MARÍA JOSÉ CORREA

M. H. Argentina S.A. Emilio Civit, 355.5500, Mendoza, Argentina

SILVIA J. AMETRANO

Department of Mineralogy, National University of La Plata, Paseo del Bosque s/n° B1900FWA, La Plata, Buenos Aires, Argentina

RICARDO O. ETCHEVERRY

Institute of Mineral Resources, National University of La Plata, 64 Street 3, B1904DZB, La Plata, and Consejo Nacional de Investigaciones Científicas y Técnicas (CONICET), Buenos Aires, Argentina

MILKA K. DE BRODTKORB

Department of Geology, University of Buenos Aires, Ciudad Universitaria, Pabellón II, C1428EHA, and Consejo Nacional de Investigaciones Científicas y Técnicas (CONICET), Buenos Aires, Argentina

ABSTRACT

The example of manganese mineralization studied in this paper makes up the major concentration of this element in Argentina. It comprises an area of 70 by 30 km in the eastern Sierras Pampeanas, located in Córdoba and Santiago del Estero provinces. It is quite unusual since it is hosted in granodioritic and rhyodacitic rocks. Geochemical, petrological and structural analyses demonstrate that these rocks are unrelated to the mineralization process. The geometry and distribution of the veins are controlled by a dextral shear system related to north–south lineaments. Textural and structural analyses of the veins indicate four different stages of mineralization. Ore minerals precipitated during the first three, whereas the gangue was mainly formed during the last stage. X-ray diffraction and electron-microprobe studies show that Mn^{4+} oxides (hollandite, pyrolusite, ramsdellite, romanèchite and cryptomelane) associated with Fe^{3+} oxides (goethite and hematite) are the main ore minerals. Calcite, opal, barite, and lesser amounts of fluorite, quartz and "chalcedony" are the most common gangue minerals. Fluid-inclusion studies show that this mineralization was associated with aqueous solutions of low salinity and a temperature of about 125°C. Isotopic analyses based on several samples of calcite ($\delta^{13}C$, $\delta^{18}O$) and barite ($\delta^{34}S$, $\delta^{18}O$) have demonstrated the dominance of meteoric waters in the hydrothermal fluids. Finally, the chemical composition of manganese oxides supports the hypothesis of an epithermal system developed in continental environments.

Keywords: manganese, epithermal deposits, Sierras Pampeanas, Ambargasta Ranges, Argentina.

SOMMAIRE

L'exemple de minéralisation en manganèse dont il est question ici constitue la plus grande concentration de Mn en Argentine. La zone minéralisée s'étend sur une superficie de 70 × 30 km dans la chaîne des Sierras Pampeanas orientales, située dans les provinces de Córdoba et de Santiago del Estero. La minéralisation y est assez inhabituelle, parce qu'elle est encaissée par des roches granodioritiques et rhyodacitiques. Les analyses géochimiques, pétrologiques et structurales démontrent que ces roches n'ont rien à voir avec la minéralisation. La géometrie et la distribution des veines sont régies par un système de failles dextrales cisaillantes liées à des linéaments nord–sud. Nos analyses texturales et structurales des veines indiquent quatre stades distincts de minéralisation. Les minéraux du minerai se sont formés au cours des trois premiers, tandis que les minéraux de la gangue se

E-mail address: leal@gl.fcen.uba.ar

sont surtout formés lors du dernier stade. Nos données obtenues en diffraction X et avec une microsonde électronique montrent que les oxydes contenant Mn^{4+} (hollandite, pyrolusite, ramsdellite, romanèchite et cryptomélane) associés aux oxydes de Fe^{3+} (goéthite et hématite) sont les principaux minéraux du minerai. Calcite, opale, barite, et des quantités moindres de fluorite, quartz et "calcédoine" sont les espèces prédominantes dans la gangue. D'après les inclusions fluides, la minéralisation était associée à des solutions aqueuses de faible salinité à une température d'environ 125°C. Les données isotopiques fondées sur plusieurs échantillons de calcite ($\delta^{13}C$, $\delta^{18}O$) et de barite ($\delta^{34}S$, $\delta^{18}O$) démontrent la dominance de l'eau météorique dans la phase fluide hydrothermale. La composition chimique des oxydes de manganèse étayent l'hypothèse d'un système épithermal développé dans un contexte continental.

(Traduit par la Rédaction)

Mots-clés: manganèse, gisements épithermaux, Sierras Pampeanas, ceinture de Ambargasta, Argentine.

Introduction

The Sierras Pampeanas ranges make up the easternmost elevation of the South American Andean orogen. In their northeast boundary, a suite of hills, called the Ambargasta Ranges, exposes an old basement mainly composed of granodiorite, granite, tonalite, dacite and rhyolite. This igneous basement occupies nearly 8,000 km^2 and is the host rock of the manganese mineralization studied in this paper. This district produced manganese from the early 1900s until 1980, when the exploitation stopped. During those years, 450,000 tonnes of mineral and about 78,400 tonnes of manganese were mined.

The genesis of the most important manganese deposits can be related to hydrothermal activity, sedimentary processes or supergene processes (Maynard 1983). The hydrothermal deposits associated with hypogene fluids, of various geological ages, probably represent analogues of recent hot spring deposits in the continents. Hewett & Fleischer (1960) recorded 0.10 to 3.4 ppm Mn in hot-spring waters in the USA responsible for the deposition of Mn oxides; these commonly show associations with fluorite, calcite, barite and travertine. The presence of W and Tl is fairly consistent in these deposits (Hewett *et al*. 1963). Enrichments of selected elements lead to the formation of cryptomelane (K), romanèchite (Ba), hollandite (Ba) and coronadite (Pb). In this type of deposit, the Mn minerals may form ore-grade concentrations or may be present as gangue species such as rhodochrosite, manganoan calcite, and kutnohorite. These deposits are rather small, and their host rocks are usually not genetically related to the orebodies. They are mostly restricted to the epithermal zone and occur as veins and irregular bodies, in some cases in breccias.

In the literature, there is not much information about manganese vein deposits occurring in granites. Hewett (1964) cited some examples in Arizona and New Mexico, and O'Reilly (1992) described the New Ross district in Lunenburg County, Nova Scotia, Canada. In Argentina, Brackebusch discovered the manganese district studied in this paper in 1893, but the first reports were published by Beder (1931) and Rayces (1947). Since then, there have been several contributions describing the mineralogy, geochemistry and the precipitation sequences from specific and restricted areas. A recent project has provided enough information to draw conclusions about the geological framework of this manganese mineralization in the Pampean Ranges in light of previous contributions (Brodtkorb & Hillar 1963, Arcidiácono 1973, Herrmann 1988, Ramè *et al*. 1999, Perri 2000, Leal 2002, Correa 2003a, Ametrano *et al*. 2005).

Here, we focus on the tectonic setting that produced the hydrothermal system, the structure, the geochemical condition during the ore precipitation, the spatial distribution of the most important minerals, and the changes in the assemblages across the evolution of this deposit. Even though most of these data have been previously published, the first holes provided us with original new evidence from the deepest level. Results of new chemical analyses from those levels, plus others as yet unpublished, allow us for the first time to attempt an explanation for the evolution of the whole mineralized system. These original data are compared with all the data taken from different sectors of this manganese deposit. We also add to this review all the isotopic studies as well as the fluid-inclusion data that have been obtained in the last four years, and already largely published. Finally, we characterize the mineralogy of manganese oxides and the sequence of their precipitation in order to determine the number of mineralization events and the compositional characteristics of each cycle of ore deposition.

The Host Rocks

There are only two units that occur as the host rocks of this manganese deposit: the Proterozoic granitic batholith and the rhyodacitic body of the Los Burros Formation. Both make up the igneous basement of Ambargasta Ranges (Fig. 1), but each one represents different stages of evolution of a Proterozoic arc.

The granitic batholith changes its composition from tonalite in the south to granite toward the north. Tonalites and granodioritic rocks are widely exposed in the southern sector, where they appear as small outcrops that usually host enclaves. Those enclaves, whose compositions range from gabbro to tonalite, have an

irregular shape, and they vary from a few millimeters to a few meters across (Lucero 1969, Castelote 1985a, Lira *et al*. 1997, Leal 2002, Miró 2005). Toward the north, the composition of the igneous basement changes gradually; granitic rocks become more common, and the number of enclaves decreases gradually.

In spite of these different mineralogical compositions, all these granitic rocks present the same geochemical signature. Trace-element profiles in different sectors of the igneous basement provide evidence that all these rocks comprise a single batholith generated in a continental volcanic arc (Bonalumi 1988, Lira *et al*. 1997, Leal 2002, Correa 2003a, Miró 2005). Most of the samples analyzed plot as I-type granites and fall within the field of metaluminous to weakly peraluminous granitic rocks (Lira *et al*. 1997, Leal 2002, Correa 2003a).

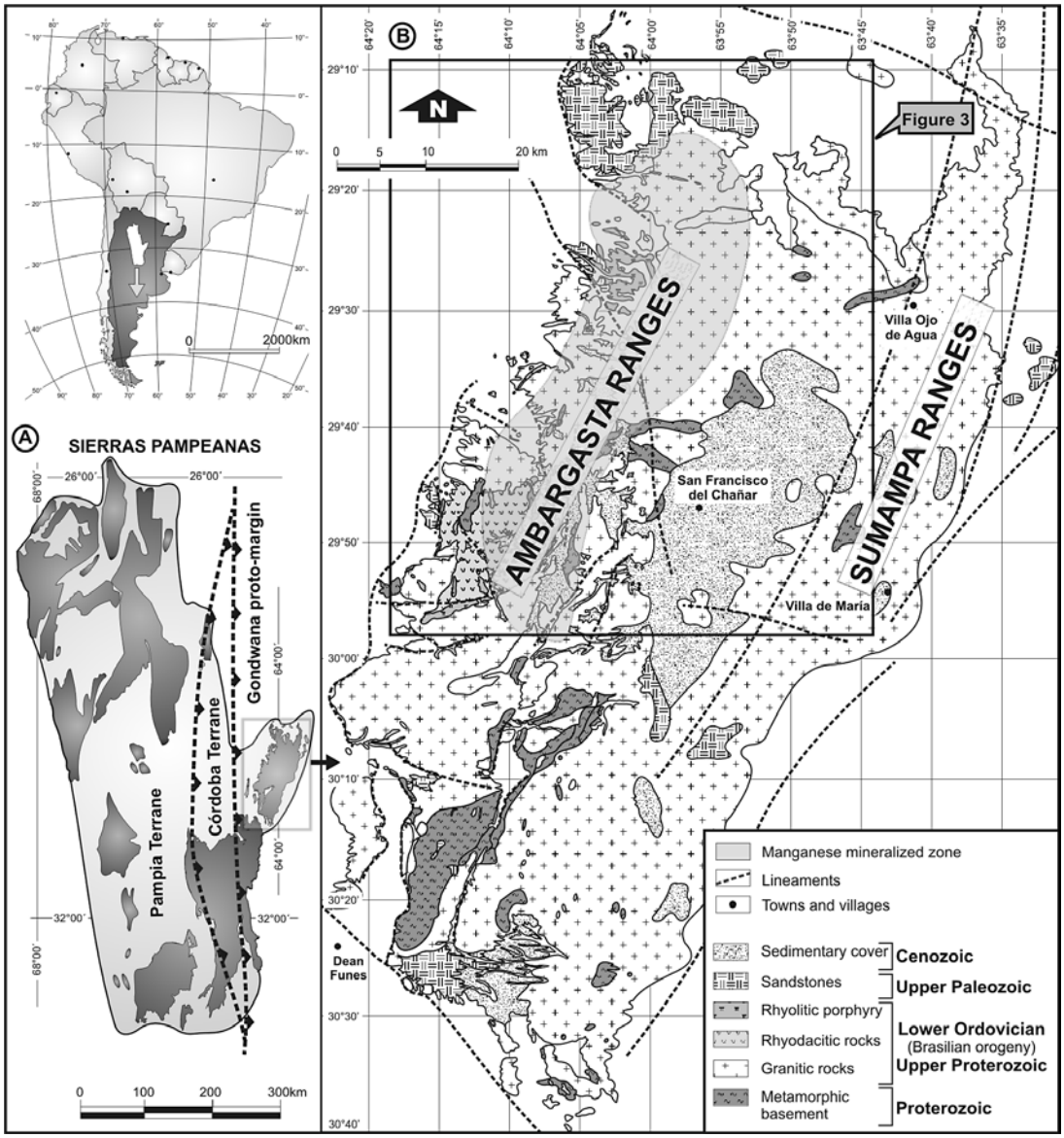

FIG. 1. Sketch of the manganese mineralized zone, location of the study area, and geological map of the eastern Sierras Pampeanas.

The Los Burros rhyodacite is a semicircular subvolcanic body that also hosts manganese veins and intrudes some of the granites previously described (Fig. 1). Its rhyodacitic to rhyolitic composition remains fairly constant, but its textures vary from porphyritic to aphanitic. Quartz, plagioclase, hornblende and biotite occur as phenocrysts in a microgranitic groundmass (Lira *et al*. 1997, Leal 2002). Chemical analyses indicate higher values of K_2O and SiO_2 compared to the surrounding granitic rocks (Lira *et al*. 1997). Although the contact with the country rocks does not crop out (it is covered by Tertiary sediments), the ages obtained show that this volcanism is somewhat younger than the granitic batholith (Leal *et al*. 2003).

All these rocks have been modified by a superimposed regional metamorphism, which caused mineralogical changes only, without significant modifications of their original chemical composition. In granodioritic rocks, biotite is transformed into chlorite, epidote and prehnite. Plagioclase and K-feldspar are usually altered to clay minerals and white micas. This regional metamorphism also affected the rhyodacite body, where it mainly produced a strong alteration of the K-feldspar present in the groundmass. This process is observed in many areas; the secondary assemblages indicate very low temperatures of alteration.

Regional Geology and Tectonic Setting

The manganese mineralization is located in the northeast boundary of the Sierras Pampeanas, where the Ambargasta Ranges are exposed with a north–south orientation (Figs. 1A, B). The evolution of this sector started in the Upper Proterozoic, when this region comprised the western margin of an old continent (Gondwana). At that time, the collision of two terranes (Córdoba and Pampia) against the Gondwana proto-margin produced an important orogeny during the Brasiliano Cycle (Ramos 1988, 1995) (Figs. 2A, B). Although its onset is still a subject of controversy, recent studies suggest that orogeny must have been between 555 and 490 Ma (Ramos *et al*. 2003, Leal *et al*. 2003, Schwartz *et al*. 2008).

The oldest rocks affected by the Brasiliano Cycle are predominantly schists, gneisses and hornfels of Proterozoic age; vestiges remain as small outcrops (Metamorphic basement: Fig. 1). Castellote (1982, 1985a, b) obtained ages between 665 ± 20 and 407 ± 10 Ma by the K/Ar method on various samples; however, these rocks usually show younger ages (Cambrian) due to overprinting by metamorphic processes.

Igneous rocks then intruded these metamorphic sequences. This igneous basement, which occupies the largest portion of the ranges, is the host rock to manganese mineralization. It is mainly composed of a batholith that varies in composition from tonalite to granite. Even though the K/Ar method yielded ages older than 700 Ma (Castellote 1985a, Linares & Gonzalez 1990), the most recent analyses obtained by SHRIMP show ages between 514 and 584 Ma (Rapela *et al*. 1998, 2007, Llambias *et al*. 2003, Miró 2005, Schwartz *et al*. 2008). Two other lithologies are associated with this magmatic event: a rhyodacitic body (Los Burros Formation) and small rhyolitic dykes (Oncán Formation) (Fig. 1). These volcanic rocks were dated by K/Ar, U/Pb on magmatic zircon and Rb/Sr methods, yielding ages between 557 and 494 Ma (Rapela *et al*.

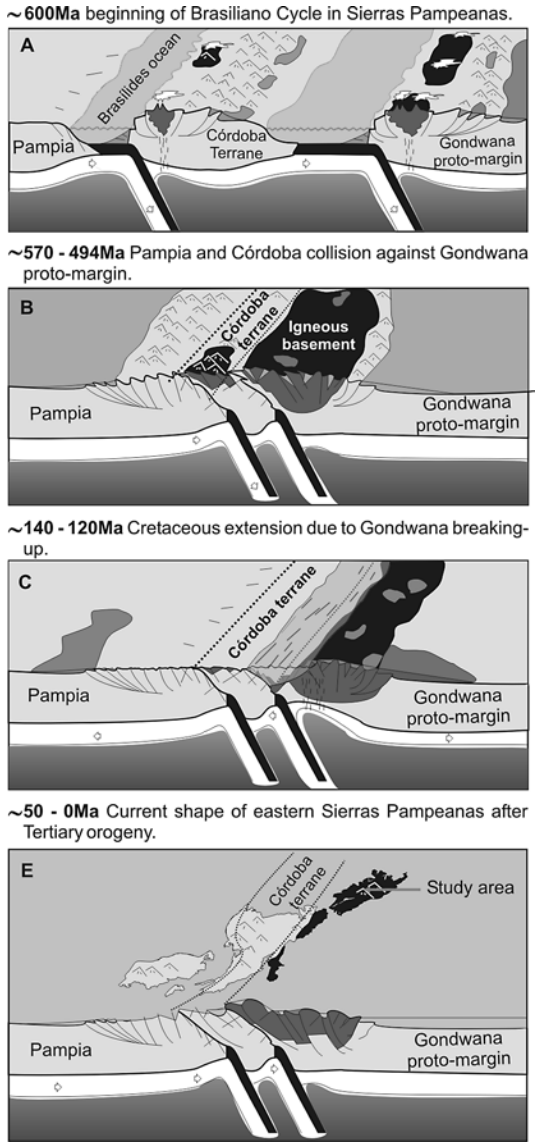

FIG. 2. Outline of the plate-tectonic evolution from the Proterozoic to the Tertiary in the eastern Sierras Pampeanas.

1991, Söllner *et al*. 2000, Ramos *et al*. 2003, Correa 2003b). On the basis of geochemical data, Lira *et al*. (1997) and Bonalumi (1988) established its affinity with an Eopaleozoic volcanic arc.

Later, during Cretaceous time, this area was subjected to extension as a result of the break-up of Gondwana (Fig. 2C). Tankard *et al*. (1995) suggested that in this period, northwest-trending dextral shear systems affected the eastern part of Argentina, including the study area. In the Ambargasta Ranges, small outcrops of red sandstones, breccias and conglomerates remain as the consequence of this extensional environment (Miró 2005). Dikes of alkali basalt a few meters wide by less than 100 meters long can be found in restricted areas cross-cutting the igneous basement. Up to now, the lack of geochronological studies on these rocks has prevented assigning an age of emplacement.

Finally, during Neogene times, the subduction of the Nazca plate under the western margin of South America caused a compressive state that structured these ranges until they developed into their current shape and size. This event only produced the uplift of basement blocks with north–south strikes without associated volcanic activity (Fig. 2E) (Ramos 1999).

A detailed documentation of the complete stratigraphy of these ranges is available in Miró (2005).

Distribution and Structures of the Manganese Veins

These deposits are made up of more than ninety veins grouped into fourteen districts (Figs. 3A, B). The most important ones, according to their yield, are the district B (Los Hoyos), district H (Aguada del Monte), district J (Los Ancoches) and district LL (El Remanso). District F (La Baritina, *i.e.,* "The Barite") is quite unusual because its veins have high concentration of gangue minerals. These five districts are the most studied areas, and several contributions have been published. The other nine districts are smaller and do not show significant differences. Beder (1931) grouped the ninety veins into three areas according to the predominance of gangue minerals: opal is the most common mineral in the northern sector, barite is mainly found in the central part, and calcite in the southern sector (Figs. 3A, B). Even though manganese minerals are present in these three areas, iron oxides seem to be concentrated only in the H district (central part, Fig. 3A).

According to recent studies of the various assemblages, this distribution of minerals suggests different levels of the same mineralized structure, which is mainly composed of N–S-trending faults cross-cutting the igneous basement subvertically (Figs. 4A, B, C). Only two of the ninety veins have a NW–SE trend (J and H districts, Fig. 3B). There are no studies to determine how deep these structures are, but it is known that some mineralized veins reach more than 300 meters in depth. Slickenside structures found in some veins show horizontal displacements associated to a dextral shear system (Ichazo 1978, Moreno *et al*. 1988, Perri 2000, Leal & Ramos 2002, Correa & Cabana 2002, Ametrano *et al*. 2005). On the basis of the distribution of veins and the kind of movements determined in most of them, we suggest that this structure was produced by Riedel deformation along a larger-scale lineament (Correa & Cabana 2002, Leal & Ramos 2002). This kind of movement could generate the morphology of "pinches and swells" that characterize the manganese veins on the surface of the study area and the stockwork textures that surround the largest ones. It is worth emphasizing that dextral shear movements are consistent with the structural style proposed by Tankard *et al*. (1995) and Rossello & Mozetic (1999) for the ranges during Cretaceous time. The age of the mineralization was a subject of controversy until Brodtkorb & Etcheverry (2000) proved, by K/Ar method on cryptomelane, that the manganese precipitation took place at 134.5 ± 3 Ma. This K/Ar dating was made in the geochronological Laboratories of the Geological Survey of Israel with the approach of Segev *et al*. (1991, 1995).

It is important to highlight that those mineralized structures do not show evidence of any kind of movement after hydrothermal deposition. Therefore, they must have remained inactive during the Tertiary orogeny. The youngest faults and lineaments are responsible for the present shape of the Ambargasta Ranges, and hence they control the exposure level of the basement. Figure 3A shows that the mineralized area is cross-cut by several regional structures with NW–SE and N–S trends. The geometry of these Tertiary lineaments allows us to explain not only the concentration of manganese veins toward the Western border of the igneous basement but also the different levels of exposure of the hydrothermal systems. According to this hypothesis, the mineralized zone only crops out toward the west of the N–S lineament because the eastern sector of the basement represents deeper levels, and manganese mineralization there could have been eroded as a result of post-Cretaceous uplift. The NW–SE structures are smaller, and therefore they expose various levels of the same mineralization. Thus, in the southern sector, the shallow portion of the systems crops out, whereas toward the north, deeper levels are exposed. For these reasons, this hydrothermal system can be divided into four different sectors (Fig. 3A) not only because they are limited by Tertiary faults but also because each area, among these structures, shows similar assemblages.

According to this scheme, the H and J districts (Figs. 3A, B) represent the deepest levels currently exposed. Therefore, three boreholes were made in these areas in order to determine how the system continues below the surface. Figure 5 shows the drill holes angled to intersect the structure at a vertical depth between 200 and 300 meters.

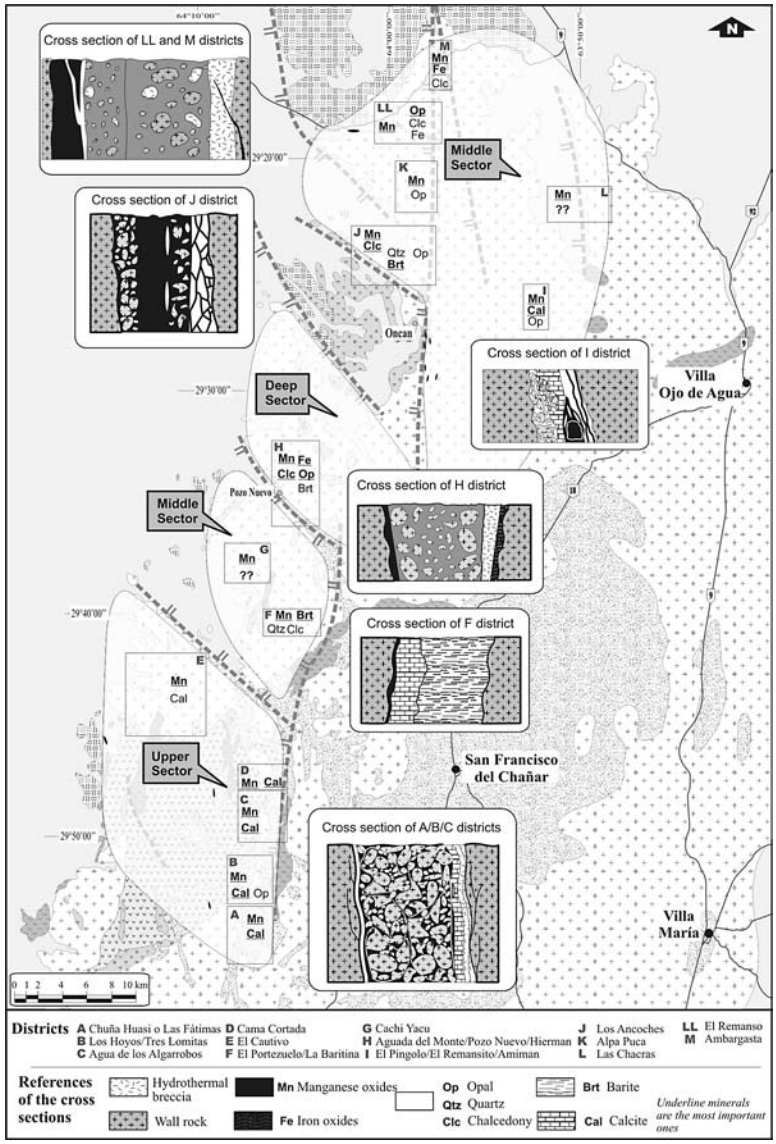

FIG. 3A. Sketch of the fourteen districts of manganese deposits that compose four different sectors. Cross sections of the most important veins are also indicated. The area of the Figure is located in the inset of Figure 1.

Across the H district (Pozo Nuevo), two holes (AMD2 and AMD3; Fig. 5A) intercepted several fault zones and breccias that mainly consist of "chalcedony", hematite and quartz. Although the mineralized structures seem to continue below 300 meters, manganese oxides that appear at the surface were not found in the drill core. On the contrary, manganese minerals were only sampled from seven to fifteen meters depth on a small shallow vein (Fig. 5A). It is important to highlight that at deeper levels, the same structure appears totally filled by iron oxides, which suggests a gradual increase in the proportion of iron oxides.

The third hole (AMD1, made in the J district; Fig. 5B) shows a similar scheme. The drill holes intercepted fault breccias that represent deeper levels of the same mineralized structure. "Chalcedony" and, to a lesser

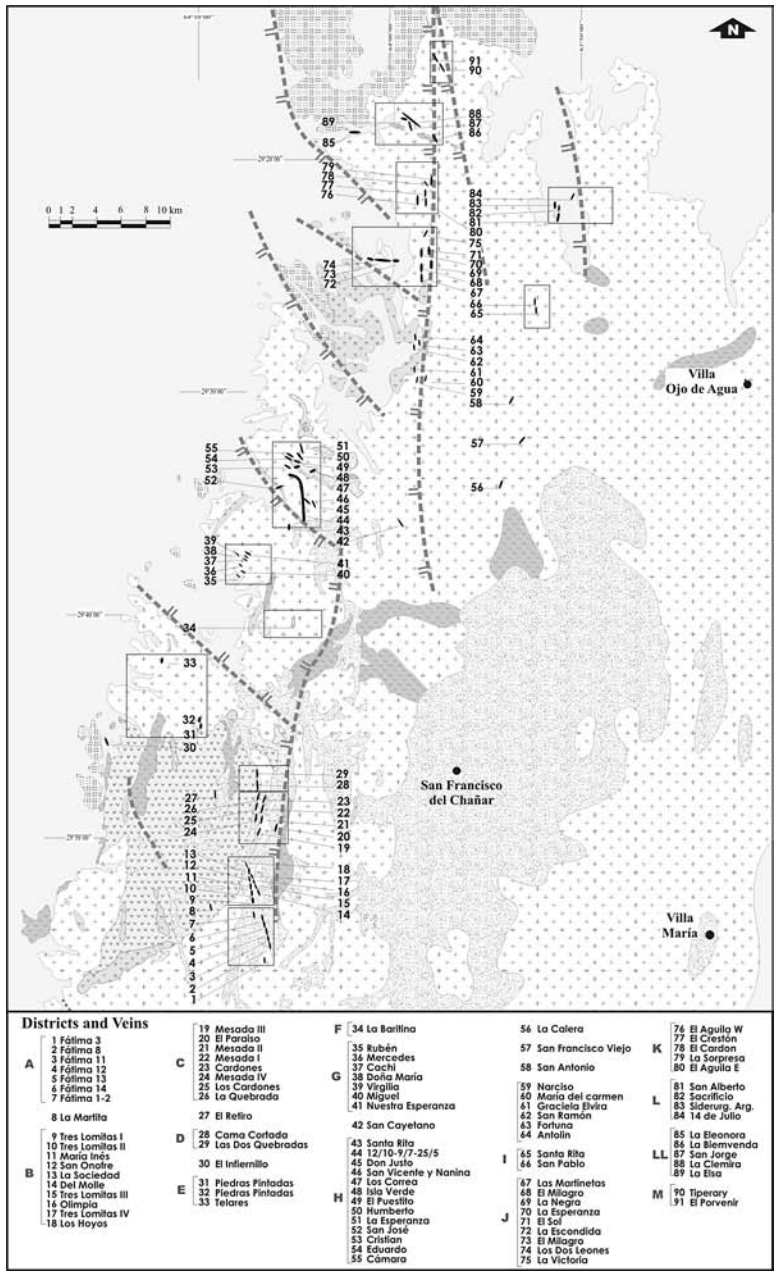

FIG. 3B. Distribution of the veins that compose the whole system of manganese mineralization. References are the same as for Figure 3A.

extent, fluorite, barite and calcite, are the minerals that fill them. Again, manganese minerals were not found at the deepest levels, where iron oxides become the matrix of the breccias.

On the basis of these data, it is possible to postulate that at least in these two districts, manganese minerals do not occur at deeper levels because they are gradually replaced by iron oxides. This replace-

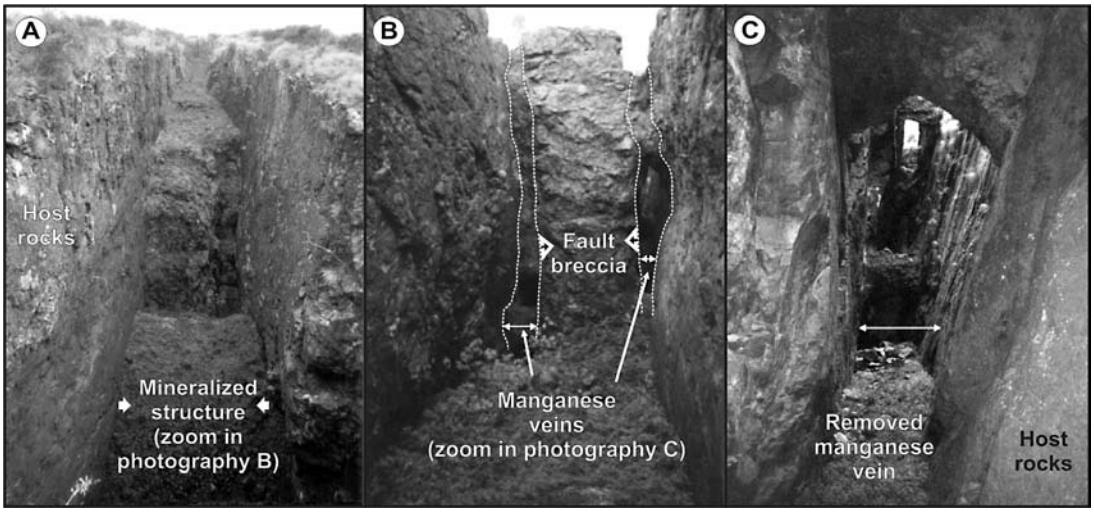

FIG. 4. A) Photo of the Tres Lomitas vein, in which fault planes in the host rock and the mineralized structure can be seen. B) Photo showing how the breccia-filled fault and the Mn-rich veins fill the mineralized structures. C) Detail of the structure that results after the exploitation of the manganese vein.

ment of ore elements suggests a REDOX gradient from deep reducing zones, rich in iron oxides, to shallow oxidizing areas, where manganese oxides become more common.

THE TEXTURES

As mentioned, manganese and iron oxides occur together filling faults, shears and breccia zones (Figs. 4B, C). Where iron oxides are absent, the veins are composed totally of Mn oxides, and *vice versa*. Most of the cross sections of the veins show a fault-breccia structure in which the metallic minerals mainly occur in the matrix (Figs. 6A, D, E). A microscope study shows that most of this matrix, as well as the breccias, is composed of small fragments of wallrock, quartz, K-feldspar crystals and earlier aggregates of Mn minerals (Fig. 6E). The competency of these breccias is dependent on the amount of silica present in the matrix. Breccias with a more siliceous matrix are extremely hard, whereas those with a matrix consisting essentially of oxides are far softer. Inside these structures, in their richest parts, there are veinlets a few centimeters wide totally filled by manganese oxides (Fig. 6C). These open cavities and the well-formed crystals provide evidence that these small fractures have been produced during the last stages of deformation. These last movements were less important than the previous ones, and thus produced small fractures only.

MINERAL COMPOSITION

Mineralogical determinations were done by X-ray diffraction, optical studies and micro-analyses. X-ray-diffraction patterns were collected between 4° and 70° 2θ in 0.05 steps using Cu*K*α radiation (50 kV, 30 mA). Electron-microprobe analyses were carried out on selected polished sections with a JEOL JXA 8900 RL instrument (25 kV) at Aachen University (Germany). With these techniques, several oxides and hydroxides were documented, among which those containing tetravalent manganese are the most common. Hollandite [$Ba(Mn^{4+},Mn^{2+})_8O_{16}$], romanèchite [$(Ba,H_2O)_2(Mn^{4+},Mn^{3+})_5O_{10}$], cryptomelane [$K(Mn^{4+},Mn^{2+})_8O_{16}$], pyrolusite [$Mn^{4+}O_2$] and ramsdellite [$Mn^{4+}O_2$] occur along the whole system as the main species (Tables 1, 2). Hollandite, cryptomelane and romanèchite are mainly present as a fine-grained mixture in banded aggregates (Figs. 6F, G). Veins filled with fine-grained crystals are common (Fig. 6G). There, romanèchite, hollandite and cryptomelane occur as a hard, dark, fine-grained mixture with a botryoidal texture. Pyrolusite and ramsdellite consist of earthy masses or well-formed crystals that reach some millimeters in length (Figs. 6H, I, J). Vugs and drusy cavities, where euhedral crystals grew, are frequently observed within these dark aggregates. These two species are less important than the other manganese oxides and are usually associated with iron oxides filling small

veinlets. Hausmannite ($Mn^{2+}Mn^{3+}{}_2O_4$), braunite ($Mn^{2+}Mn^{3+}{}_6SiO_{12}$), manganite [$Mn^{3+}O(OH)$], lithiophorite [$(Al,Li)Mn^{4+}O_2(OH)_2$], nsutite [$Mn^{2+}{}_xMn^{4+}{}_{1-x}O_{2-2x}(OH)_{2x}$], todorokite [$(Mn^{2+},Ca,Mg)Mn^{4+}{}_3O_7 \cdot H_2O$] and coronadite [$Pb(Mn^{4+},Mn^{2+})_8O_{16}$] have been described also as minor species by Arcidiácono (1973). However, these last seven species were determined considering their optical properties only, but their presence could not be confirmed either through X-ray diffraction or micro-analyses in the samples studied. Coronadite is the only one that can be present as a minor component of fine-grained mixtures owing to the anomalies of lead detected in some of the analyzed sections.

Goethite is the most common iron oxide; it usually occurs together with hematite. Magnetite, partially replaced by hematite, has been mentioned in the H district (Figs. 3A, B) only; it occurs as a minor species (Ramè *et al*. 1999, Ametrano *et al*. 2005). These iron oxides mainly appear as aggregates with a botryoidal

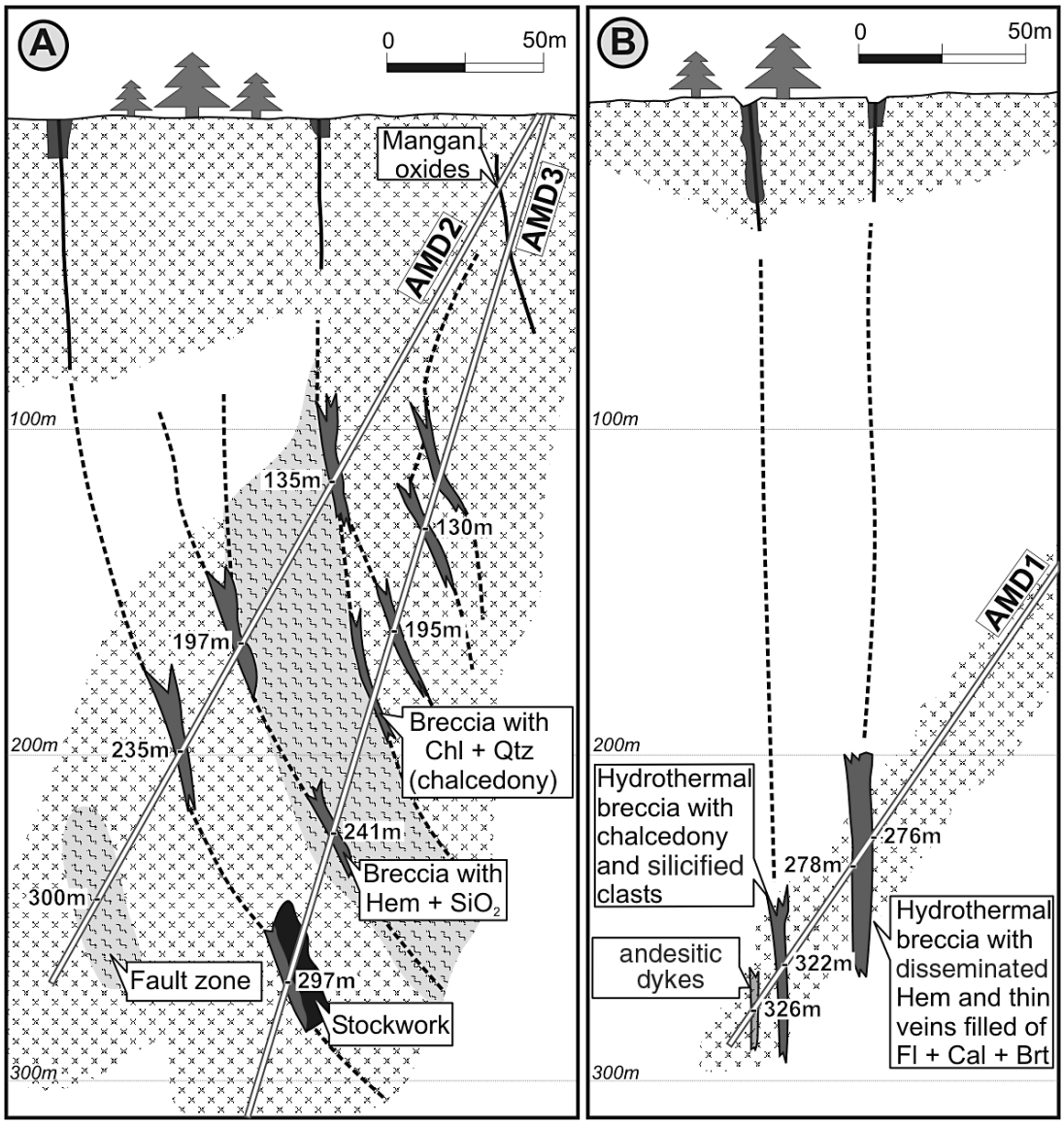

FIG. 5. Sketch of the boreholes in district H (A: Pozo Nuevo) and district J (B: La Santiagueña).

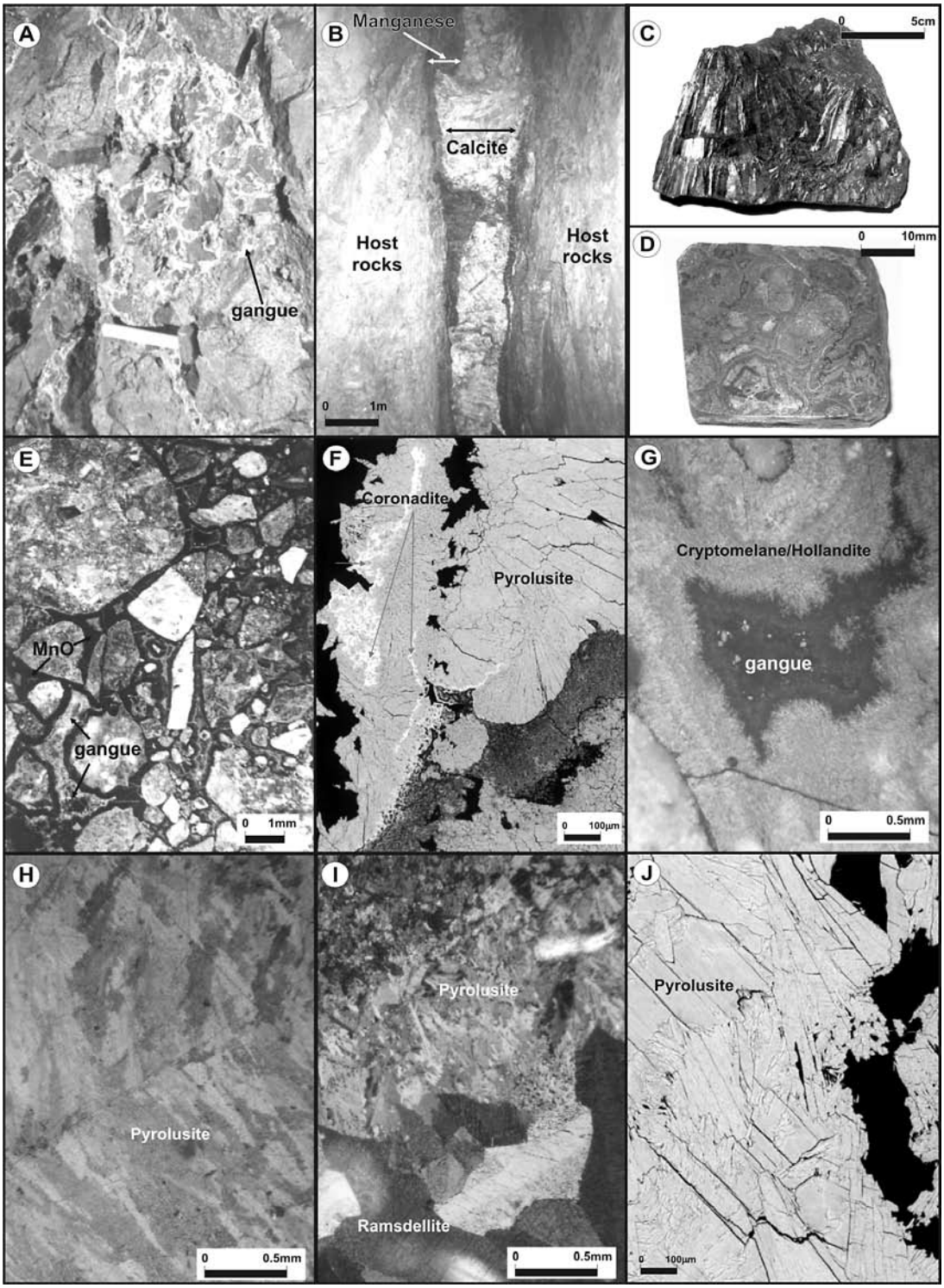
A
gangue
B
Manganese
Calcite
Host rocks
Host rocks
0 1m
C
0 5cm
D
0 10mm
E
MnO
gangue
0 1mm
F
Coronadite
Pyrolusite
0 100µm
G
Cryptomelane/Hollandite
gangue
0 0.5mm
H
Pyrolusite
0 0.5mm
I
Pyrolusite
Ramsdellite
0 0.5mm
J
Pyrolusite
0 100µm

texture filling veins, together with manganese oxides. They may form iron-rich veins without any other species, but they mainly appear as microscopic aggregates associated with the manganese oxides.

According to Arcidiácono (1973), Herrmann (1988) and Ramè *et al*. (1999), gold was observed in a few samples in association with those metallic minerals. However, as this mineral is determined by its optical properties in polished sections only, up to now, we can rule out the presence of native gold. Our mineralogical studies, as well as the chemical analyses done in several samples, suggest that native gold did not crystallize in the shallow levels of the structure that are exposed at present. Perhaps the grains described by our colleagues represent one of the species at deeper levels. In this case, the samples taken from the boreholes suggest that the crystallization of gold must have taken place 300 meters below the surface.

Gangue minerals can be found in the breccia matrix, as massive veins or as thin films (Figs. 6A, B, C). The maximum size of calcite veins is 10 meters long by 7 meters wide and 1 meter thick (D district, Figs. 3A, B). In these veins, calcite appears as rhombic crystals larger than ten centimeters. Vugs and drusy cavities commonly contain fluorite and barite as fine-grained masses (A district, Figs. 3A, B). The fluorite crystals are smaller than two millimeters, but barite ranges from a few millimeters to some centimeters in length. Different colors of opal can be found as thin films overgrowing other minerals or filling thin veins. Chemical analyses of several samples of opal were performed by Correa (1998), but no evident relation between their color and their composition was established. "Chalcedony" also occurs covering the surface of larger crystals in the open cavities. Quartz is completely absent or restricted to microscopic crystals associated with the manganese oxides.

Distribution of Ore and Gangue Minerals

There is a geographic distribution of the species previously described, along the 70 km of this manganese-rich belt as a result of the levels of exposure of the system. Although manganese oxides are species that occur in similar proportions in all the districts, as Arcidiácono (1973) pointed out, there is a slight increase in cryptomelane toward the north, whereas hollandite becomes more abundant in the southern sectors. Iron oxides are particularly important in the H district (Figs. 3A, B), where they occur in similar proportions to manganese species. This anomaly in the amount of iron is one of the reasons why we believe that this district represents the deepest level of the system. In the other districts, iron oxides are among the minor species, and in some of them (A–F districts, Figs. 3A, B), they may be absent. The northern sector also contains iron oxides, but in this area, they appear as local anomalies (LL district, Fig. 3B).

Along the whole system, non-metallic minerals precipitated at the same time (during the last stages of the hydrothermal process), but different species characterize each area. Varieties of silica are the most common in the northern sector, in which opal composes the matrix of the breccias and fills most of the cavities. "Chalcedony", quartz and barite are less common minerals. Within this northern sector, calcite is only important in district "I" (Fig. 3B), where it is as abundant as opal (Perri 2000). Conversely, in the southern sector, the gangue consists predominantly of calcite. Fluorite, barite, varieties of silica and clay minerals are ubiquitous locally. Finally, districts G and F (Figs. 3A, B) show unusual assemblages of gangue minerals. In district F, barite, the most abundant species, fills veins several centimeters wide. There, tabular crystals reach five centimeters long and usually form a cockscomb texture. Open spaces between barite crystals were filled by calcite and opal, which become more common toward the end of the mineralization event (Leal & Gonzalez 2008). "Chalcedony" and quartz only occur inside a few small cavities as minor species.

The Paragenetic Sequence

The great extent of Mn mineralization and its restricted exposure (owing to the extensive Quaternary sediments) make it difficult to establish a precise paragenetic sequence of all the minerals previously described. However, the data compiled from more than 60 veins allow us to propose an order of precipitation of the minerals (Fig. 7). Two different kinds of textures suggest two main conditions of precipitation. The earliest structures and the most important ones are characterized by fault breccias whose matrix is mainly composed of metallic minerals (manganese and iron oxides). The spatial association of these species and the breccia structures suggest that during the precipitation of the ore, the fluids must have ascended through fault structures generated at the same time or shortly before the hydrothermal processes started. Although it has long been recognized that the whole process of precipitation took place in different events according to the general

FIG. 6. A) Breccia structure in which the matrix is composed of ore and gangue minerals. B) Vein structure filled by manganese aggregates and calcite. C) Ramsdellite aggregates from a manganese vein. D–E) Microbreccia textures with manganese oxides and gangue minerals in the matrix. F) Back-scattered electron image illustrating assemblages of pyrolusite and coronadite. G) Polished section of cryptomelane and hollandite aggregates. H) Polished section of pyrolusite. I) Polished section of pyrolusite and ramsdellite. J) Back-scattered electron image of pyrolusite aggregates.

TABLE 1. INFORMATION ON MINERALOGY, FLUID INCLUSIONS, STABLE ISOTOPES AND REFERENCE FOR EACH DISTRICT

District	Ore minerals	Gangue minerals	Fluid inclusions	$\delta^{13}C_{PDB}$	$\delta^{18}O_{PDB}$	$\delta^{18}O_{SMOW}$	$\delta^{34}S_{CDT}$	References
A	**hollandite**, **pyrolusite**, **romanèchite**, cryptomelane	**calcite**, barite, *fluorite*	T_h = 100°C T_e = -22°C -1.6 < $T_{m(ice)}$ < -2.4°C 2.7 < Sal. < 4 wt% NaCl eq	-2.1 -1.1 -4.1 -1.2	-8.2 -10.5 -7.1 -9.9	22.4 20.0 23.5 20.7	 4.9 7.7	Leal (2002)
B	**hollandite**, **pyrolusite**, **romanèchite**, cryptomelane, hausmannite, manganite, jacobsite, lithiophorite, goethite	**calcite**, opal, *barite*, *fluorite*, *braunite*		-2.7 -0.6 0.02 -3.0	-9.7 -10.1 -9.1 -10.5	20.9 20.4 21.5 20.0		Rayces (1947) Ramè *et al.* (1999), Leal (2002)
C	**hollandite**, **pyrolusite**, **romanèchite**, cryptomelane	**calcite**						Leal (2002)
D	**hollandite**, **romanèchite** pyrolusite, cryptomelane	**calcite**		-0.2 -1.8	-9.5 -9.5	21.1 21.1		Ramè *et al.* (1999), Leal (2002)
E	**romanèchite**, pyrolusite,	**calcite**, *opal*, "*chalcedony*"	undetermined					Beder (1931)
F	romanèchite, *pyrolusite*	**barite**, opal, **calcite**, quartz, *fluorite*	T_h = 148°C T_e = -32°C $T_{m(ice)}$ = -3.2°C Sal. = 5.1% NaCl eq	-18.4	11.9	6.5		Leal & González (2009)
G	unknown	unknown	undetermined					
H	**hollandite**, **romanèchite**, **pyrolusite**, **cryptomelane**, manganite, todorokite, nsutite, ramsdellite, woodruffite, lithiophorite, goethite, hematite, magnetite, *ilmenite*	**opal**, "**chalcedony**", barite, calcite	undetermined	-8.6 -8.4 -5.1 -5.0 -9.0	-9.8 -8.5 -8.8 -8.9 -10.7	20.8 22.2 21.2 21.7 19.8		Sánchez Rial y Centeno (1987) Ramè *et al.* (1999) Ametrano *et al.* (2005)
I	**hollandite**, romanèchite, pyrolusite	**calcite**, opal, "chalcedony", *fluorite*	undetermined					Perri (2000)
J	**hollandite**, **ramsdellite**, **cryptomelane**, **romanèchite**, pyrolusite, coronadite, goethite, hematite	**opal**, "**chalcedony**", quartz, calcite, barite, *fluorite*	undetermined					Arcidiácono (1973)
K	**romanèchite**	**opal**	undetermined					Beder (1931)
L	**romanèchite**	**opal**, "chalcedony"	undetermined					Beder (1931)
LL	**cryptomelane**, **romanèchite**, hollandite, pyrolusite, ramsdellite, coronadite, goethite, hematite	**opal**, "chalcedony", quartz, calcite, *barite*, *fluorite*	T_h = 105°C T_e = -38°C -1.5 < $T_{m(ice)}$ < -3°C 3.86 < Sal. < 5.14 wt% NaCl eq	-3.8	-9.6	21.0	6.8	Arcidiácono (1973), Correa (1998, 2003a)
M	**cryptomelane**, **romanèchite**, hollandite, pyrolusite, ramsdellite, coronadite, **goethite**, hematite	**opal**, "**chalcedony**", quartz, calcite, *barite*, *fluorite*						Correa (2003a)

The data on fluid inclusions acquired in district A apply also to districts B, C and D; the data on fluid inclusions acquired in district LL apply also to district M. Names of minerals shown in bold-face font indicate the most abundant species, whereas those shown in italics are present in minor proportions only. "Chalcedony" is shown in quotation marks because it is a mixture and not the name of a mineral species.

compositional features of the breccias, four main stages can be established. The first one is characterized by red breccias whose matrix is completely filled by iron oxides (Stage 1, Fig. 7). The second and the most important one gave the fault breccias composed of manganese oxides and lesser amount of other minerals (Stage 2, Fig. 7). They are the largest structures that resulted from the most important episode of compressive deformation. Following smaller fractures that result from the last movement that affected these structures is the third stage (Stage 3, Fig. 7). It is important to highlight that even though during this stage the amount of ore minerals was smaller, the veinlets produced at that stage are the richest ones.

Later, when the compressive stresses decreased, most of these fault structures collapsed and produced new channels for fluid rise. Gangue minerals that precipitated formed symmetrical banding textures with evidence of open spaces (Stage 4, Fig. 7). Thus the irregular distribution of gangue minerals along the whole system may have been controlled not only by the level of exposure but also by the evolution of the structure at the end of the mineralization. The open cavities in veins several centimeters wide, which are common in the southern and middle sectors, could have been produced owing to the geometric arrangement between the mineralized fault-planes and the strains. According to this hypothesis, the southern sector, where calcite, barite and opal are more abundant species than manganese and iron oxides, could have been the sector where the collapse of the structures produced easier channels for the rapid rise of the hydrothermal solutions.

Geochemistry of the Ore Minerals

Several chemical analyses of manganese oxides were performed to establish the environment of precipitation, its properties and the amount of trace elements. Special care was taken to obtain pure samples. These concentrates were obtained by separating aggregates of manganese oxides by hand, under a binocular microscope. Their purity was checked by X-ray diffraction. Concentration of major and trace elements were established by using inductively coupled plasma (ICP), whereas Au and Ag were also measured by fire-assay fusion, atomic absorption spectroscopy (AA) and gravimetric methods. Table 3 shows the average composition of manganese oxides from the most important districts.

TABLE 2. REPRESENTATIVE COMPOSITIONS OF THE MOST IMPORTANT MANGANESE-BEARING SPECIES

	Rmn	Cpt	Hol	Hol	Pyl–Rmd	Pyl–Rmd
SiO_2 wt%	b.d.	0.90	0.12	0.28	b.d.	b.d.
Al_2O_3	b.d.	0.28	0.28	0.28	b.d.	b.d.
MgO	0.06	0.05	0.01	0.02	b.d.	b.d.
Na_2O	0.04	b.d.	b.d.	b.d.	0.68	0.10
BaO	17.57	2.77	14.72	15.30	0.01	0.01
MoO_3	b.d.	b.d.	b.d.	b.d.	0.01	0.02
MnO_2	79.83	86.89	76.99	76.02	93.40	96.81
NiO	b.d.	b.d.	b.d.	b.d.	0.01	0.01
SrO	b.d.	b.d.	b.d.	b.d.	0.19	0.07
PbO	b.d.	b.d.	b.d.	b.d.	0.02	0.04
Fe_2O_3	0.74	1.48	1.25	1.40	0.10	0.21
ZnO	b.d.	b.d.	b.d.	b.d.	0.13	0.10
K_2O	0.11	5.39	0.41	0.11	2.42	0.11
WO_3	0.13	b.d.	b.d.	b.d.	0.01	0.02
Total	98.42	97.76	93.78	93.42	97.00	97.52
Si *apfu*	--	0.11	0.02	0.04	--	--
Al	--	0.04	0.04	0.05	--	--
Mg	0.00	0.01	0.00	0.00	--	--
Na	0.01	--	--	--	0.02	0.00
Ba	0.58	0.13	0.81	0.84	0.00	0.00
Mo	--	--	--	--	0.00	0.00
Mn	4.67	7.47	7.43	7.39	0.98	1.00
Ni	--	--	--	--	0.00	0.00
Sr	--	--	--	--	0.00	0.00
Pb	--	--	--	--	0.00	0.00
Fe	0.05	0.14	0.13	0.15	0.00	0.00
Zn	--	--	--	--	0.00	0.00
K	0.01	0.86	0.07	0.02	0.05	0.00
W	0.00	--	--	--	0.00	0.00

b.d.: below the detection limit (0.01 wt%) of the electron microprobe used. The compositional data are recalculated into atoms per formula unit on the basis of the following number of atoms of oxygen per formula unit: 10 (romanèchite, Rmn), 16 [cryptomelane (Cpt), hollandite (Hol)], and 2 [pyrolusite (Pyl), ramsdellite (Rmd)].

TABLE 3. AVERAGE COMPOSITION OF POLYMINERALIC SAMPLES OF MANGANESE OXIDES FROM THE MOST IMPORTANT DISTRICTS

District #	A 2	B 4	C 5	D 3	H 19	H 5	LL 24
Name	*Chuña Huasi*	*Los Hoyos*	*Agua de los Algarrobos*	*Cama Cortada*	*Pozo Nuevo surface*	*Pozo Nuevo boreholes*	*El Remanso*
Mn	>20000	>20000	>20000	>20000	>20000	42190	365440
Fe	1.17	0.35	0.49	0.24	0.06	4.74	0.75
Al	1.40	0.20	0.31	0.21	0.03	5.52	0.77
Na	0.15	0.14	0.11	0.10	0.01	1.60	0.08
K	1.19	0.71	0.18	0.14	0.03	3.77	0.98
Mg	<0.01	<0.01	<0.01	<0.01	<0.01	<0.01	0.01
Ca	3.78	1.45	2.16	3.35	1.33	3.04	0.35
Ti	<0.01	<0.01	<0.01	<0.01	<0.01	0.14	0.00
S	0.05	0.04	0.05	0.06		0.08	0.05
P						270.2	
Cu	1305.0	859.5	3951.2	6790.0	78.5	152.6	162.4
Ni	26.0	27.5	24.0	19.3	6.1	6.3	0.8
Co	19.0	104.2	114.6	248.7	17.4	16.3	39.4
Zn	131.5	658.0	252.6	224.3	45.6	57.7	183.5
Pb	574.5	1250.0	6381.2	1524.3	211.2	250.4	1477.0
Ba	>2000	1716.0	>2000	>2000	>2000	14226.6	> 2000
Sr	2000.0	1667.2	1887.4	2000.0	536.9	274.9	3281.2
V	410.5	465.7	404.0	448.0	371.8	136.9	227.8
Mo	23.5	275.7	53.0	69.7	18.5	18.9	127.5
Li	21.5	16.5	93.6	30.7	6.7	41.9	19.9
Zr	5.0	19.2	3.2	0.3	2.3	44.2	2.7
Y	31.5	46.7	29.4	18.3	26.7	20.7	36.6
As	188.5	205.2	277.4	233.7	155.3	50.3	118.1
Cd	<0.2	0.7	<0.2	<0.2	<0.2	<10	<0.2
W	595.0	243.2	200.2	175.3	164.7	134.3	776.9
Bi	9.0	13.7	13.2	15.3	<5	25.0	21.8
Sb	44.0	52.0	33.8	<5.0	58.2	25.0	113.8
Te	<10	<10	<10	<10	<10	<100	<10
Cr	<1.0	3.5	21.0	<1.0	26.6	6.2	32.6
Sn	<20	<20	<20	<20	<20	100	<20
La	85.5	34.2	288.6	199.0	69.0	57.0	75.7
Ga	<2.0	27.7	16.0	5.7	21.8	10.0	19.9
Nb	37.5	43.0	37.4	41.0	29.7	5.0	14.8
Sc	<5	<5	<5	<5		<50	<5
Ta	<10	<10	<10	<10	<10	<100	57.4
Hg					0.002	1.0	
Au	20.5	7366.0	167.6	10.7	7.6	5.0	26.9
Ag	<0.2	49.8	<0.2	<0.2	<0.02	2.5	31.7

References: districts A, B, C and D: Leal (2002), H (from the surface): Ametrano *et al.* (2005), H (from boreholes): this work, LL: Correa (2003a). * Concentrations of Fe, Mg, Al, Na, K, Ca, Ti and S are expressed in wt%, whereas the amount of Au is expressed in ppb, and that of the rest of the elements is expressed in ppm.

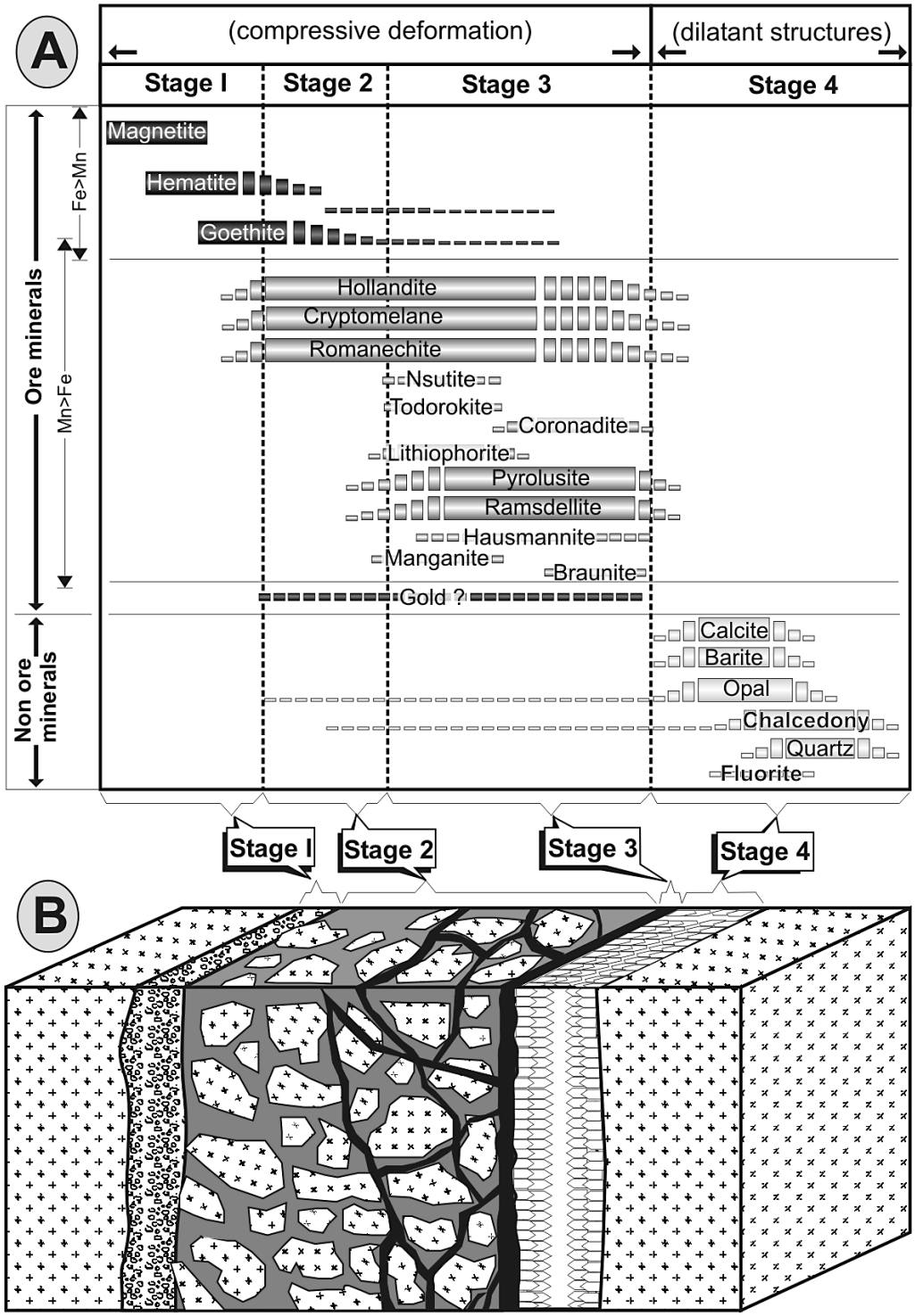

FIG. 7. A) Paragenetic sequence for the four stages of mineralization. B) Cross-section showing the relationship between each stage and the mineralized structures.

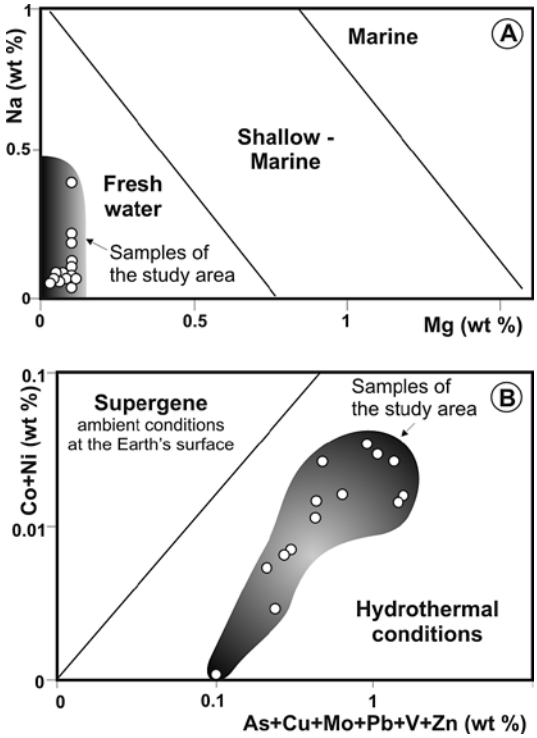

FIG. 8. Geochemical signature of the manganese oxides. (A) Freshwater signature, (B) hydrothermal conditions.

As was pointed out by Nicholson (1992), the high amount of some elements, such as Ba, Cu, Li, Mo, Pb, Sr, V and Zn, provides evidence of the role of hydrothermal solutions. On the other hand, the presence of W, As and Sb, which has been already noted in previous studies (Arcidiácono 1973, Brodtkorb & Hillar 1964), suggests that the hydrothermal systems could have been linked to magmatic fluids (Hewett *et al*. 1963). Some of the elements permit differentiation between manganese oxides formed in fresh water, shallow-marine and marine environment, whereas others distinguish between manganese oxides formed on the Earth's surface under ambient conditions and those precipitated at deeper levels (Nicholson 1992). For the manganese deposits described in this paper, the oxides must have precipitated in a continental environment (Fig. 8A) under hydrothermal conditions (Fig. 8B). This environment is also consistent with the $^{87}Sr/^{86}Sr$ values obtained in some samples of manganese oxides, which are constrained between 0.70711 and 0.71177, consistent with an association with continental crust.

Gold was only detected in high amounts (20.6 ppm: Leal 2002) in samples from the Los Hoyos district (Fig. 3A). This element is usually associated with silver anomalies, which are more common in the central sectors. As is the case here, silver is commonly absorbed or probably incorporated in the structure of manganese oxides.

Finally, the amount of Pb in some ore samples suggests the presence of coronadite; however, it has not been confirmed by X-ray studies.

FLUID INCLUSIONS AND STABLE ISOTOPES

In order to establish the temperature of the crystallization, several contributions of fluid-inclusion studies were carried out in the last five years. As the manganese and iron oxides are not amenable to this kind of analysis, it was done with gangue minerals. Although calcite, fluorite and mainly barite are considered unreliable species to use this method, special care was taken to measure primary fluid inclusions. Thus, the temperature obtained for the crystallization of these minerals concurs with those determined in quartz. The minerals studied were sampled from the most important districts and were studied with Chaixmeca and Linkam stages calibrated with synthetic fluid inclusions (Table 1). In the southern sector, these analyses have been made on calcite, barite and a few crystals of fluorite (Leal 2002). These species host different types of fluid inclusions, among which only those that occur as isolated individuals or in random groups were inferred to be primary. On the contrary, fluid inclusions aligned along microfractures in transgranular trails were designated as secondary; they were not measured. Primary monophase liquid inclusions with no vapor bubble (observed at 25°C) are frequently found in these minerals, whereas two-phase inclusions (with a liquid:vapor ratio ≥ 2) represent about 30%. They present both regular and irregular shapes, and may show negative crystal forms. The sizes of these primary inclusions range from 10 to 200 μm. Most assemblages homogenize to liquid at temperatures less than 100°C, but values attain temperatures of about 200°C. Average temperatures of final melting of ice ($T_{m\ ice}$) fall in a narrow range from –1.6 and –2.4°C . From these results, the estimated salinities fall in a range from 2.7 to 4 wt% NaCl equiv. Microthermometric results from this sector are summarized in Table 1.

Microthermometric analyses were also done in district F where barite, calcite and quartz are more abundant than ore minerals (Leal & González 2009). Here, even though secondary fluid-inclusions are the most common ones, primary fluid-inclusions can be found as isolated individuals of regular shapes that reach 70 μm in diameter. These inclusions homogenize to liquid at about 140°C, which suggests temperatures slightly higher than those obtained in the other districts (Table 1). The average eutectic temperatures (T_e) was determined to be –32°C, whereas melting temperatures of ice ($T_{m\ ice}$) were about –3°C. These results suggest

hydrothermal solutions composed of NaCl, $MgCl_2$ and $CaCl_2$ in concentrations lower than 5 wt% NaCl equiv.

Finally, in the northern sector, fluid-inclusion studies show similar results, but in this case, most of the data were obtained from quartz crystals, which are more reliable than the other species analyzed (Correa 2003a). With this mineral, two families of homogenization temperatures (T_h) allowed us to determine two different kinds of inclusions. The first group was obtained from inclusions with stretching and necking down; their values of T_h (higher than 170°C) were not considered as reliable data. On the contrary, the second family is composed of primary inclusions with homogenization temperatures of about 105°C. Salinities range from 3.9 to 5.1 wt% NaCl equiv. (with a few values of about 8 wt% NaCl equiv.), which indicate values slightly higher than other minerals of the same district. Eutectic temperatures (–38° to –30°C) could be measured in few inclusions, and therefore a precise mode could not be established. The large ratio and values close to –35°C suggest fluids in the system NaCl–$MgCl_2$–H_2O (Davis *et al*. 1990) or NaCl–H_2O with the presence of additional cations like $CaCl_2$ or $MgCl_2$ (Table 1).

Stable isotopes have been also analyzed in gangue minerals. Several samples of calcite were collected to measure $\delta^{13}C$ and $\delta^{18}O$, whereas $\delta^{34}S$ was established with barite crystals. The $\delta^{18}O$ data are reported on the Vienna standard mean ocean water (V–SMOW) and the Pee Dee Formation Belemnite (PDB); the $\delta^{13}C$ and $\delta^{34}S$ values are reported with respect to the PDB and CDT (Canyon Diablo troilite), respectively (Table 1). The $\delta^{13}C$ and $\delta^{34}S$ values obtained in all analyzed samples are consistent with carbonates and sulfates precipitated from fresh water (Hoefs 1997).

According to the oxygen isotope exchange-coefficient for calcite and water (Kim & O'Neil 1997) and temperatures of fluid-inclusion homogenization in calcite (100°C), the original solutions yield $\delta^{18}O$ values between 3.9 and 7.38‰, which is characteristic of meteoric waters (Hoefs 1997).

Thus, fluid-inclusion studies show that this system, at least during the precipitation of the gangue minerals, maintained a temperature of about 100°C. Boiling processes thus must not have taken place during this last stage. The low salinities and the isotopic data compiled support the hypothesis of hydrothermal fluids were associated with meteoric waters.

The Alteration of the Surrounding Veins

Although the process of manganese mineralization affected an area seventy kilometers long by thirty kilometers wide, it did not produce a strong alteration of the igneous basement (Fig. 1B). In fact, the alteration can only be determined by optical studies of samples taken from near the largest Mn veins (the first 10 meters), in which the granitic rocks underwent deformation of quartz and K-feldspar. In these sectors, several networks of millimeter-wide veinlets, filled by opal, quartz and K-feldspar (adularia habit), usually appear. Calcite and minor epidote were found in a few restricted areas (Perri 2000, Leal 2002, Correa 2003a). This alteration grades outward to white mica – chlorite zone and usually into unaltered host-rocks. The weak alteration related to the mineralization shows that the hydrothermal fluids must have circulated at low temperatures, as corroborated by the fluid-inclusion analyses.

In a few cases, episyenites are observed in the granitic walls of some veins. Desilication is only present in the first two or three centimeters, where the wallrock keeps its original texture with pitted vugs due to complete leaching of primary quartz. However, as the vugs remained open, we infer that this alteration process occurred later and should not be associated with manganese mineralization.

Discussion

The source of manganese is the most puzzling aspect of these deposits; mineralization appears in an area without important concentrations of this element. Most of the manganese deposits are linked to mafic or ultramafic rocks that have higher concentration of this element (Wedepohl 1972). However, in the Sierras Pampeanas, these vein deposits are hosted in a granitic batholith without any evidence of a manganese anomaly. Some years ago, mineralization was attributed to a Tertiary orogeny that produced sparse basalts toward the west of the studied area. The lack of superimposed deformation supports this hypothesis, but the Cretaceous age obtained by Brodtkorb & Etcheverry (2000) forced us to discard this idea. In that period, several basalts were produced owing to the break-up of Gondwana. A possible source could thus be the release of Mn and Fe from basic rocks that are overlain by the Tertiary sediments, through which hydrothermal fluids must have circulated. Another source could be related to the mafic and ultramafic rocks that remained from the subduction of ocean crust below the Gondwana protomargin during the Pampean orogeny. If the source of this element was actually located to the west, this hypothesis would account for the presence of manganese veins only along the western boundary of the Ambargasta Ranges.

On the other hand, from our present knowledge, the hypothesis of gold concentration at deeper levels cannot be supported. Some chemical analyses and optical observations suggest the presence of Au as local anomalies in the southern sector. However, there is not enough information from the deepest sectors of the mineralization to confirm this assumption.

Conclusions

All evidence compiled in the last five years suggests that the formation of the manganese mineralization was generated in Cretaceous times and therefore is younger than the igneous basement. At that time, these rocks underwent strong deformation due to the breakup of Gondwana. Hence, north–south lineaments and several faults were produced, among which those that produced open spaces useful for the upward movement of fluid.

Ore minerals were formed at deeper levels than the gangue species. Manganese and iron oxides were precipitated when the solution reached oxidizing conditions, whereas the gangue minerals formed at shallower levels, owing to a temperature decrease or local changes in pH. Hollandite, cryptomelane, romanèchite, pyrolusite and ramsdellite are the main manganese oxides present in this deposit. According to Roy (1968) and Nicholson (1992), these Mn^{4+} oxides are usually formed in epithermal systems near the surface, where the amount of oxygen is high and the temperature is low. Even though we have observed that in the first meters of this deposit, the ore minerals are invariably Mn^{4+} oxides, reduced species with Mn^{3+}, Mn^{2+} and iron oxides appear commonly at deeper levels. On the other hand, the geographic distribution of calcite, barite and opal suggest that during the last stage, the conditions were not exactly the same along the whole mineralized area.

The limited alteration produced by the mineralization event on the wallrocks and the temperature determined by fluid-inclusion studies indicate hydrothermal fluids with low temperatures (~100°C). Interaction between the host rocks and the mineralization seems to be restricted to sparse veinlets filled by opal, quartz, K-feldspar of adularia habit, calcite and epidote.

There is no evidence that allows us to determine the exact depth at which mineralization runs out; however, all the compiled data suggest that it might continue at the deeper levels; therefore, the manganese concentration generated from the hydrothermal process could be greater than previous estimates.

Finally, the evolution of the mineralization process can be divided into four main stages. The veins started as a transtensive structure but finished dominated by extensional collapse. At the beginning, during the first three events, the ore minerals precipitated as the main species, but at the end, the gangue minerals were predominant.

Acknowledgements

Many thanks to the University of La Plata, the University of Buenos Aires, and CONICET for supporting this project, and M. H. Argentina S. A. for allowing us to publish the information obtained during the course of their drilling campaign. The authors are grateful to the referees and the Editor for their helpful suggestions and discussions.

References

Ametrano, S., Etcheverry, R. & Tessone, M. (2005): Análisis químico y metalogenético del grupo minero Hiermang (Mn–Fe), provincia de Córdoba. *16° Congreso Geológico Argentino* **2**, 791-798.

Arcidiácono, E.C. (1973): Génesis de yacimientos de óxidos de manganeso de Ojo de Agua, Santiago del Estero, República Argentina. *Revista de la Asociación Geológica Argentina* **28**, 165-194.

Beder, R. (1931): Los yacimientos de minerales de manganeso en el norte de la provincia de Córdoba y sur de Santiango del Estero. *Anal. Mus. Nac. Hist. Nat.* **36**.

Bonalumi, AA. (1988): Características petrológicas y geoquímicas de los granitoides asociados a la mineralización de manganeso en el norte de la provincia de Córdoba y sur de Santiago del Estero, República Argentina. 5° Congreso Geológico Chileno **2**, 47-61.

Brodtkorb, M.K. & Etcheverry, R. (2000): Edad K/Ar de la mineralización de manganeso de Aguada del Monte, provincia de Córdoba. *Revista de la Asociación Geológica Argentina* **55**(3), 280-283.

Brodtkorb, M.K. & Hillar, N. (1963): Hallazgo de ramsdellita en la República Argentina. *II Jornadas Geológicas Argentinas* **2**, 35-40.

Castellote, P. (1982): La formación La Clemira y edad de su metamorfismo. *Acta Geológica Lilloana* **16**(1), 71-76.

Castellote, P. (1985a): Algunas observaciones geológicas en las sierras de Ambargasta y Sumampa (provincia de Santiago del Estero). *Acta Geológica Lilloana* **16**(2), 259-269.

Castellote, P. (1985b): La formación "Pozo del Macho", integrante del basamento metamórfico de la sierra de Ambargasta, provincia de Santiago del Estero. *Acta Geológica Lilloana* **16**(2), 275-280.

Correa, M.J. (1998): Geoquímica de las fases silíceas de la veta La Clemira, distrito manganesífero El Remanso, provincia de Santiago del Estero. *4° Reunión de Mineralogía y Metalogenia*, 43-49.

Correa, M.J. (2003a): *La mineralización de manganeso en el distrito minero El Remanso y sus relaciones metalogenéticas, Sierras Pampeanas Orientales, Santiago del Estero*. Tesis doctoral de la Universidad Nacional de La Plata, Buenos Aires, Argentina.

Correa, M.J. (2003b): Petrología y edad K/Ar de diques relacionados a la formación Oncán, sierras de Ambargasta, Santiago del Estero. *Revista de la Asociación Geológica Argentina* **58**(4), 664-668.

CORREA, M.J & CÁBANA, M.C. (2002): Análisis estructural de la veta La Clemira, Sierra de Ambargasta, Santiago del Estero. VI Congreso de Mineralogía y Metalogenia (Buenos Aires), 111-114.

DAVIS, D.W., LOWENSTEIN, T.K. & SPENCER, R.J. (1990): Melting behavior of fluid inclusions in laboratory-grown halite crystals in the systems NaCl–H_2O, NaCl–KCl–H_2O, NaCl–$MgCl_2$–H_2O, and NaCl–$CaCl_2$–H_2O. *Geochim. Cosmochim. Acta* **54**, 591-601.

HERRMANN, C.J. (1988): *Geología económica del yacimiento "Tres Lomitas", departamento de Sobremonte, provincia de Córdoba*. Thesis, Universidad de Buenos Aires, Argentina.

HEWETT, D.F. (1964): Veins of hypogene manganese oxide minerals in the southwestern United States. *Econ. Geol.* **59**, 1429-1472.

HEWETT, D.F. & FLEISCHER, M. (1960): Deposits of manganese oxides. *Econ. Geol.* **55**, 1-55.

HEWETT, D.F., FLEISCHER, M. & CONKLIN, N. (1963): Deposits of the manganese oxides: supplement. *Econ. Geol.* **58**, 1-51.

HOEFS, J. (1997): *Stable Isotope Geochemistry* (4th ed.). Springer-Verlag. Berlin, Germany.

ICHAZO, G.J. (1978): Control tectónico de la mineralización de manganeso en la sierra de Ambargasta, Santiago del Estero. *Revista de la Asociación Geológica Argentina* **33**, 345-354.

KIM, S.T. & O'NEIL, J.R. (1997): Equilibrium and nonequilibrium oxygen isotope effects in synthetic carbonates. *Geochim. Cosmochim. Acta* **61**, 3461-3475.

LEAL, P.R. (2002): *Estudio metalogenético de los yacimientos de manganeso del departamento de Sobremonte, provincia de Córdoba, sierras Pampeanas Orientales*. Tesis doctoral de la Universidad Nacional de La Plata, Buenos Aires, Argentina.

LEAL, P.R. & GONZALEZ, M.P. (2009): Mineralogía e inclusiones fluidas en La Baritina: tope de la mineralización de manganeso más importante de la Argentina, sierras de Ambargasta, provincia de Córdoba. *Revista de la Asociación Geológica Argentina* (in press).

LEAL, P.R., HARTMANN, L.A., SANTOS, J.O.S., MIRÓ, R.C. & RAMOS, V.A. (2003): Volcanismo postorogénico en el extremo norte de las Sierras Pampeanas Orientales: nuevos datos geocronológicos y sus implicancias tectónicas. *Revista de la Asociación Geológica Argentina* **58**(4), 593-607.

LEAL, P.R. & RAMOS, V.A. (2002): Marco estructural asociado a vetas de manganeso del norte de la provincia de Córdoba. *XV Congreso Geológico Argentino* **I**, 3-9.

LINARES, E. & GONZÁLEZ, R.R. (1990): Catálogo de edades radiométricas de la República Argentina, años 1957-1987. *Asociación Geológica Argentina, Publicación Especial*.

LIRA, R., MILLONE, H.A., KIRSCHBAUM, A.M. & MORENO, R.S. (1997): Calc-alcaline arc granitoid activity in the Sierra Norte – Ambargasta ranges, central Argentina. *J. S. Am. Earth Sci.* **10**, 157-177.

LLAMBIAS, E.J., GREGORI, D., BASEI, M.A., VARELA, R. & PROXY, C. (2003): Ignimbritas riolíticas neoproterozoicas en la sierra Norte de Córdoba: ¿evidencia de un arco magmático temprano en el ciclo Pampeano? *Revista de la Asociación Geológica Argentina* **58**(4), 572-582.

LUCERO, H.N. (1969): Descripción geológica de las hojas 16h (Pozo Grande) y 16i (Chuña Huasi), provincia de Córdoba y Santiago del Estero. *Boletín de la Direc. Nac. Geol. Min.* **107**.

MAYNARD, J.B. (1983): *Geochemistry of Sedimentary Ore Deposits*. Springer Verlag, Berlin, Germany.

MIRÓ, R.C. (2005): Hoja Geológica 2963-III, Villa Ojo de Agua, provincias de Santiago del Estero y Córdoba. *Secretaría de Minería de la Nación, Boletín* **315**.

MORENO, R., BONALUMI, A. & MILLONE, H. (1988): Estudio petroestructural del distrito manganesífero de Pozo Nuevo, departamento de Sobremonte – provincia de Córdoba. *V Reunion de Microtectónica*, 51-56.

NICHOLSON, K. (1992): Contrasting mineralogical–geochemical signatures of manganese oxides: guides to metallogenesis. *Econ. Geol.* **87**, 1253-1264.

O'REILLY, G.A. (1992): Petrographic and geochemical evidence for a hypogene origin of granite-hosted, vein-type Mn mineralization at the New Ross Mn deposits, Lunenburg County, Nova Scotia, Canada. *Econ. Geol.* **87**, 1275-1300.

PERRI, M. (2000): Caracterización geológica–metalogénica del distrito manganesífero Amimán. Santiago del Estero. *V Congreso de Mineralogía y Metalogenia*, 401-407.

RAMÈ, G.L., LIRA, R. & GAY, H.D. (1999): La mineralización de manganeso del norte de Córdoba. *XIV Congreso Geológico Argentino, Actas* **2**, 306-309.

RAMOS, V.A. (1988): Late Proterozoic – Early Paleozoic of South America, a collisional history. *Episodes* **11**(3), 168-174.

RAMOS, V.A. (1995): Sudamérica: un mosaico de continentes y océanos. *Ciencia Hoy* **6**(32), 24-29.

RAMOS, V.A. (1999): Las provincias geológicas del territorio argentino. *In* Geología Argentina (R. Caminos, ed.). *Anales* **29**(3), 41-96.

RAMOS, V., LEAL, P.R. & HARTMANN, L.A. (2003): The northern sector of eastern Sierras Pampeanas: a key region to understand the late Proterozoic western margin of Río de La Plata cratón. *I Encontro sobre a Estratigrafía do Rio Grande do Sur: Escudo e Bacias* (Porto Alegre).

RAPELA, C.W., PANKHURST, R.J. & BONALUMI, A.A. (1991): Edad y geoquímica del pórfiro granítico de Oncan, sierra Norte de Córdoba, Sierras Pampeanas, Argentina. *VI Congreso Geológico Chileno*, 19-22.

RAPELA, C.W., PANKHURST, R.J., CASQUET, C., BALDO, E., SAAVEDRA, J., GALINDO, C. & FANNING, M. (1998): The Pampean Orogeny of the southern proto-Andes: Cambrian continental collision in the Sierras de Córdoba. *In* The Proto-Andean Margin of Gondwana (R.J. Pankhurst & C.W. Rapela, eds.). *Geol. Soc., Spec. Publ.* **142**, 343-367.

RAPELA, C.W., PANKHURST, R.J., CASQUET, C., FANNING, C.M., BALDO, E.G., GONZÁLEZ-CASADO, J.M., GALINDO, C. & DAHLQUIST, J. (2007): The Río de la Plata craton and the assembly of SW Gondwana. *Earth-Sci. Rev.* **83**, 49-82.

RAYCES, E.C. (1947): Los yacimientos de manganeso de Chuña Huasi. *Revista de la Asociación Geológica Argentina* **2**, 240-256.

ROSSELLO, E. & MOZETIC, M.E. (1999): Caracterización estructural y significado geotectónico de los depocentros cretácicos continentales del centro-oeste Argentino. *Boletín do 5° Simposio sobre o Cretáceo do Brasil*, 107-113.

ROY, S. (1968): Mineralogy of the different genetic types of manganese deposits. *Econ. Geol.* **63**, 760-786.

SÁNCHEZ RIAL, J.E. & FERREIRA CENTENO, J.P. (1987): Prospección condicionada de minerales de manganeso, Pozo Nuevo, Córdoba, Argentina. *X Congreso Geológico Argentino* **2**, 181-182.

SCHWARTZ, J.J., GROMET, L.P. & MIRÓ, R. (2008): Timing and duration of the calc-alkaline arc of the Pampean Orogeny: implications for the Late Neoproterozoic to Cambrian evolution of western Gondwana. *J. Geol.* **116**, 39-61.

SEGEV, A., HALICZ, L., LANG, B. & STEINITZ, G. (1991): K/Ar dating of manganese minerals from the Eisenbach region, Black Forest, southern Germany. *Schweiz. Mineral. Petrogr. Mitt.* **71**, 101-114.

SEGEV, A., HALICZ, L., STEINITZ, G. & LANG, B. (1995). Post-depositional processes on a buried Cambrian sequence in southern Israel, north Arabian Massif: evidence from new K/Ar dating of Mn-nodules. *Geol. Mag.* **132**, 375-385.

SÖLLNER, F., LEAL, P.R., MILLAR, H. & BRODTKORB, M.K. DE (2000): Edades U/Pb en circones de la riodacita de la sierra de Ambargasta, provincia de Córdoba. *V Congreso de Mineralogía y Metalogenia*, 465-469.

TANKARD, A.J., ULIANA, M.A., WELSINK, H.J., RAMOS, V.A., FRANCA, A.B., MILANI, E.J., BRITO NEVES, B.B., EYLES, N., SKARMETA, J., SANTA ANA, H., WIENS, F., CIBIÁN, M., LOPEZ PAULSE, O., GERMS, G.J.B., DE WIT, M.J., MACHACHA, T. & MILLER, R.McG. (1995): Structural and tectonic controls of basin evolution in southwestern Gondwana during the Phanerozoic. *In* Petroleum Basins of South America. *Am. Assoc. Petroleum Geol., Mem.* **62**, 5-52.

WEDEPOHL, K.H. (1972): Manganese. *In* Handbook of Geochemistry II-3. Springer-Verlag, Berlin, Germany.

Received January 29, 2008, revised manuscript accepted July 15, 2008.